Electron-impact ionization of the C atom

Sh. A. Abdel-Naby, C. P. Ballance, T. G. Lee, S. D. Loch, and M. S. Pindzola
Department of Physics, Auburn University, Auburn, Alabama 36849, USA

(Received 5 November 2012; revised manuscript received 23 January 2013; published 20 February 2013)

Time-dependent close-coupling (TDCC), *R*-matrix-with-pseudostates (RMPS), and time-independent distorted-wave (TIDW) methods are used to calculate electron-impact ionization cross sections for the carbon atom. The TDCC and RMPS results for the $1s^22s^22p^2$ ground configuration are in reasonable agreement with the available experimental measurements, while the TIDW results are 30% higher. Ionization of the $1s^22s2p^3$ excited configuration is performed using the TDCC, RMPS, and TIDW methods. Ionization of the $1s^22s^22p3l$ ($l = 0$–2) excited configurations is performed using the TDCC and TIDW methods. The ionization cross sections for the excited configurations are much larger than for the ground state. For example, the peak cross section for the $1s^22s^22p3p$ excited configuration is an order of magnitude larger than the peak cross section for the $1s^22s^22p^2$ ground configuration. The TDCC results are again found to be substantially lower than the TIDW results. The ionization cross-section results will permit the generation of more accurate, generalized collisional-radiative ionization coefficients needed for modeling moderately dense carbon plasmas.

DOI: 10.1103/PhysRevA.87.022708 PACS number(s): 34.80.Dp

I. INTRODUCTION

The ITER tokamak, currently under construction in Cadarache, France, will have carbon components in parts of its divertor. The impurity transport of carbon on existing tokamaks has also been an area of much study [1,2]. The use of *SXB* (effective ionization rate coefficient divided by effective photon emissivity coefficient) ratios has allowed diagnostics of the impurity influx of C using the C I 657.8-nm line [3]. We note that these *SXB* ratios require ionization rate coefficients, which should include the contribution of ionization from the excited states. However, no nonperturbative ionization cross-section calculations have been performed for excited states of neutral carbon. Hence, one of the purposes of this study is to improve the quality of the excited-state ionization cross-section data, for use in such impurity influx studies. Carbon ionization is also used in impurity transport codes, such as SOLPS [4,5], to track the amount of carbon being transported into the core region [6], a critical consideration to ensure that the power loss from the impurities does not quench the fusion reaction. At tokamak densities, it is expected that excited-state ionization would also be important for such modeling.

The importance of excited-state ionization for light species has been demonstrated on a number of occasions. The contribution to the total ionization due to collisional excitation followed by collisional ionization can often be comparable with the contribution from the ground-state ionization. For example, Loch *et al*. [7] showed that the effective ionization for neutral Li was dominated by the contribution from the excited states. Measurements from the DIII-D tokamak [8] found good agreement with the theoretical results [7]. Ionization from metastable levels played a part in resolving discrepancies in astrophysical observations of Li-like emission [9].

Previous calculations for the electron-impact ionization of C are limited to the ground state. For example, the Born-Ochkur approximation has been used to calculate ground-state ionization of C [10,11]. Other calculations were carried out [12,13] using the Born approximation. All these previous calculations have a higher total cross section when compared with the available experimental measurements of C [14], except the results of McGuire [12], where good agreement was found in the high-energy range. Also, semiempirical and empirical calculations for the ground state of C are available [15–18].

An earlier time-dependent close-coupling (TDCC) calculation for the electron-impact ionization of C [19] was limited to the ionization of the $2p$ subshell at higher energies. Reasonable agreement with the experimental measurements [14] was obtained, when these results were combined with a time-independent distorted-wave (TIDW) calculation for the ionization of the $2s$ subshell. In this paper, we extend the TDCC calculation for the direct ionization of the $1s^22s^22p^2$ ground configuration, including ionization of both the $2s$ and $2p$ subshells at low energies. We also calculate the electron-impact direct ionization of the $1s^22s2p^3$ and $1s^22s^22p3l$ ($l = 0$–2) excited configurations of C. The *R*-matrix-with-pseudostates (RMPS) method is used to calculate total electron-impact ionization cross sections from the $1s^22s^22p^2\ ^3P$ term and the lowest $^5S, ^3D$, and ^3P LS terms of the $1s^22s2p^3$ excited configuration, while the TIDW method is used to calculate total-ionization cross sections of the $1s^22s^22p^2$ ground, $1s^22s2p^3$ and $1s^22s^22p3l$ excited configurations of C. The data produced in these calculations along with other previous work on electron-impact ionization for the ground and excited states of C^+ [20,21], C^{2+} [22,23], and C^{3+} [24,25] will be used to produce more accurate generalized collisional-radiative (GCR) ionization coefficients needed for modeling of moderately dense carbon plasmas.

The rest of this paper is organized as follows. In Sec. II, we give a brief review of the theoretical methodologies used to calculate the electron-impact ionization of C. In Sec. III, we present the ionization cross-section results for the ground and excited configurations of C. We conclude with a brief summary and future plans in Sec. IV. Unless otherwise stated, we will use atomic units.

II. THEORETICAL METHODS

A. Time-dependent close-coupling method

The nonperturbative TDCC method [26] has been used to calculate electron-impact direct-ionization cross sections

for many light atoms and their ions. The two-active-electron six-dimensional wave function is expanded in coupled spherical harmonics and substituted into the time-dependent Schrödinger equation to yield a set of (l_1,l_2) close-coupled equations for each LS symmetry given by

$$i\frac{\partial P^{LS}_{l_1l_2}(r_1,r_2,t)}{\partial t} = T_{l_1l_2}(r_1,r_2)P^{LS}_{l_1l_2}(r_1,r_2,t), + \sum_{l_1',l_2'} V^{L}_{l_1l_2,l_1'l_2'}(r_1,r_2)P^{LS}_{l_1'l_2'}(r_1,r_2,t)\,, \quad (1)$$

where $T_{l_1l_2}(r_1,r_2)$ is a sum over one-electron operators for the kinetic energy and atomic core interaction, while $V^{L}_{l_1l_2,l_1'l_2'}(r_1,r_2)$ is a two-active-electron interaction operator.

The initial $t=0$ condition for the TDCC equations is a product of a bound radial orbital and a Gaussian radial wave packet. After time propagation of the TDCC equations, partial scattering probabilities $\mathcal{S}(l_1l_2LS)$ are obtained by projection of the $P^{LS}_{l_1l_2}(r_1,r_2,t\to\infty)$ radial wave functions onto antisymmetrized products of bound and continuum radial orbitals. The direct-ionization cross section is given by

$$\sigma = \frac{\pi w_0}{4(2l_0+1)k_i^2}\sum_{LS}(2L+1)(2S+1)\sum_{l_1,l_2}\mathcal{S}(l_1l_2LS), \quad (2)$$

where w_0 is the occupation number of the target subshell, $(n_0l_0)^{w_0}$, and $k_i^2/2$ is the incident energy.

The bound radial orbitals needed to construct the atomic core interaction potentials are calculated using a Hartree-Fock (HF) atomic structure code [27]. The bound and continuum radial orbitals needed for the initial $t=0$ condition and the calculation of the scattering probability $\mathcal{S}(l_1l_2LS)$ are obtained by diagonalization of the one-electron operators, making use of a pseudopotential method.

B. *R*-matrix-with-pseudostates method

The nonperturbative RMPS method [28] has been used to calculate electron-impact total-ionization cross sections for many atoms. In our implementation of the RMPS method, the basis used to represent the $(N+1)$-electron continuum was made orthogonal to the pseudo-orbitals using a method developed by Gorczyca and Badnell [29]. The scattering calculation was performed with a set of parallel R-matrix programs [24,30,31], which are extensively modified versions of the serial RMATRIX I programs [32].

R-matrix theory dictates that the configuration space describing the scattering processes is split into two regions. In the inner region, which encompasses the N-electron target, the total wave function for a given LS symmetry is expanded in basis states given by

$$\Psi_k^{N+1} = A\sum_{i,j} a_{ijk}\,\psi_i^{N+1}\frac{u_{ij}(r_{N+1})}{r_{N+1}} + \sum_i b_{ik}\,\chi_i^{N+1}, \quad (3)$$

where A is an antisymmetrization operator, ψ_i^{N+1} are channel functions obtained by coupling N-electron target states with the angular and spin functions of the scattered electron, $u_{ij}(r)$ are radial continuum basis functions, and χ_i^{N+1} are bound functions, which ensure completeness of the total wave function. The coefficients a_{ijk} and b_{ik} are determined by diagonalization of the total $(N+1)$-electron Hamiltonian. In the outer region, the total wave function for a given $LS\Pi$ symmetry is expanded in basis states given by

$$\Psi_k^{N+1} = \sum_i \psi_i^{N+1}\frac{F_i(r_{N+1})}{r_{N+1}}. \quad (4)$$

The radial continuum functions $F_i(r)$ are obtained by solving the coupled differential equations given by

$$[T_i(r) + V_{ij}(r)]F_i(r) = 0\,, \quad (5)$$

where $T_i(r)$ is a kinetic and nuclear energy operator and $V_{ij}(r)$ is an asymptotic coupling operator. For RMPS ionization calculations, the total-ionization cross section is derived from the sum of excitation cross sections from the initial term to those pseudostates lying above the ionization limit.

C. Time-independent distorted-wave method

The perturbative TIDW method [33] has been used to calculate electron-impact excitation and ionization cross sections for many atoms and their ions. The configuration-average excitation cross section is given by

$$\sigma_{\rm exc} = \frac{8\pi}{k_i^3k_f}(w_1+1)(4l_2+3-w_2)\sum_{l_i,l_f}(2l_1+1)(2l_f+1) \times \mathcal{S}(n_1l_1k_il_i\to n_2l_2k_fl_f), \quad (6)$$

where w_1 and w_2 are final-state occupation numbers, n_1l_1 and n_2l_2 are quantum numbers of the bound electrons, and k_il_i and k_fl_f are quantum numbers for the initial and final continuum electrons. The configuration-average ionization cross section is given by

$$\sigma_{\rm ion} = \frac{32w_0}{k_i^3}\int_0^{E/2}\frac{d(k_e^2/2)}{k_ek_f}\sum_{l_i,l_e,l_f}(2l_i+1)(2l_e+1)(2l_f+1) \times \mathcal{S}(n_0l_0k_il_i\to k_el_ek_fl_f), \quad (7)$$

where w_0 is an initial state occupation number, n_0l_0 are quantum numbers of the bound electron, k_il_i, k_el_e, and k_fl_f are quantum numbers of the incident, ejected, and final continuum electrons, and $E=\frac{k_e^2}{2}+\frac{k_f^2}{2}$. First-order perturbation theory is used to derive the partial scattering probabilities $\mathcal{S}(n_1l_1k_il_i\to n_2l_2k_fl_f)$ for excitation and $\mathcal{S}(n_0l_0k_il_i\to k_el_ek_fl_f)$ for ionization.

The bound radial orbitals needed for the calculations of the scattering probabilities are obtained by using a Hartree-Fock relativistic (HFR) atomic structure code [34]. The continuum radial orbitals needed for the calculations of the scattering probabilities are obtained by solving the radial Schrodinger equation. Two TIDW approaches may be used for the ionization cross sections. In the first one, the incident, ejected, and scattered electrons are all evaluated in a V^{N-1} potential [35]. In the second one, the incident and scattered electrons are evaluated in a V^N potential and the ejected electrons are evaluated in a V^{N-1} potential, where N is the number of electrons in the initial target configuration [36]. Results from the latter method will be presented. The total-ionization cross section is a sum of all excitation cross sections to configurations that can autoionize TIDW(ex) and all ionization cross sections. For neutral atoms the autoionization branching ratios are assumed to be one.

D. *LS*-term selective ionization

TDCC and TIDW direct-ionization cross sections between initial and final configurations may be easily used to calculate individual $L_iS_i \rightarrow L_fS_f$ term selective direct-ionization cross sections via a simple scaling of ionization potentials and appropriate branching ratio [37]. For transitions

$$(n_1l_1)^{w_1}L_iS_i \rightarrow (n_1l_1)^{w_1-1}L_fS_f, \tag{8}$$

where all the remaining inactive subshells are closed, the branching ratio is given by

$$B(L_iS_i \rightarrow L_fS_f) = \left[c\left(l_1{}^{w_1-1}\, L_fS_f|\right\}l_1^{w_1}L_iS_i\right)\right]^2, \tag{9}$$

where c is a coefficient of fractional parentage. On the other hand, for transitions

$$\begin{aligned}&[(n_1l_1)^{w_1}L_1S_1(n_2l_2)^{w_2}L_2S_2]L_iS_i\\ &\quad\rightarrow [(n_1l_1)^{w_1-1}L_1'S_1'(n_2l_2)^{w_2}L_2S_2]L_fS_f,\end{aligned} \tag{10}$$

with all the remaining inactive subshells closed, the branching ratio is given by

$$\begin{aligned}B(L_iS_i \rightarrow L_fS_f) &= (2L_1+1)(2S_1+1)(2L_f+1)(2S_f+1)\\ &\times \left[c\left(l_1{}^{w_1-1}L_1'S_1'\right|\}l_1^{w_1}L_1S_1\right)\right]^2\\ &\times \begin{Bmatrix} l_1 & L_1' & L_1\\ l_2 & L_i & L_f\end{Bmatrix}^2 \begin{Bmatrix} 1/2 & S_1' & S_1\\ S_2 & S_i & S_f\end{Bmatrix}^2.\end{aligned} \tag{11}$$

Therefore

$$\begin{aligned}&\sigma(L_iS_i \rightarrow L_fS_f)\\ &\quad= B(L_iS_i \rightarrow L_fS_f)\frac{I(C_i \rightarrow C_f)}{I(L_iS_i \rightarrow L_fS_f)}\sigma(C_i \rightarrow C_f),\end{aligned} \tag{12}$$

where $I(L_iS_i \rightarrow L_fS_f)$ and $I(C_i \rightarrow C_f)$ are ionization potentials for LS terms and configurations, respectively, while $\sigma(L_iS_i \rightarrow L_fS_f)$ and $\sigma(C_i \rightarrow C_f)$ are cross sections for LS terms and configurations, respectively. We note that TIDW excitation cross sections between initial and final configurations may not be used to calculate individual $L_iS_i \rightarrow L_fS_f$ term selective-excitation cross sections. Excitation cross sections are to specific final n_2l_2 bound orbitals, while direct-ionization cross sections sum over all ejected k_el_e continuum orbitals.

III. RESULTS

TDCC calculations were carried out for the electron-impact direct ionization of the $1s^22s^22p^2$, $1s^22s2p^3$, and $1s^22s^22p3l$ ($l = 0$–2) configurations of C. The energy spectrum of C was obtained by diagonalization of the one-electron Hamiltonian optimized on HF removal energies, with the introduction of $l = 0$ pseudopotentials to remove the problem of deexcitation to filled subshells [38]. The configuration-average ionization potential energies for the $2p$ subshell of the $1s^22s^22p^2$ and $1s^22s2p^3$ configurations are 10.0 and 9.3 eV, respectively. Also, the configuration-average ionization potentials for the $3s$,$3p$, and $3d$ subshells of the $1s^22s^22p3l$ ($l = 0$–2) excited configurations are found to be 3.5 eV, 2.5 eV, and 1.5 eV, respectively. These values are in reasonable agreement with their corresponding experimental measurements [39].

For the ionization of the $2s$ and $3s$ subshells, the possible LS symmetries are $(nskl)^{1,3}L$ ($n = 2,3$), with $L = l$, while in the case of the ionization of the $2p$ and $3p$ subshells, the possible LS symmetries are $(npks)^{1,3}P$ and $(npkl)^{1,3}L$ ($n = 2,3$), with $l-1 \leqslant L \leqslant l+1$ for $l \geqslant 1$. On the other hand, for the ionization of the $3d$ subshell, the possible LS symmetries are $(3dks)^{1,3}D$, $(3dkp)^{1,3}L$ ($L = 1,2,3$), and $(3dkl)^{1,3}L$, with $l-2 \leqslant L \leqslant l+2$ for $l \geqslant 2$. The number of coupled channels per LS symmetry ranged from 9 for $(2sks)$ and $(3sks)^{1,3}S$ to 30 for $(2ski)$ and $(3ski)^{1,3}I$, from 8 for $(2pkp)$ and $(3pkp)^{1,3}P$ to 30 for $(2pkj)$ and $(3pkj)^{1,3}I$, and from 8 for $(3dkp)^{1,3}P$ to 30 for $(3dkj)^{1,3}L$. The TDCC calculations were carried out for all LS symmetries with $0 \leqslant l \leqslant 7$, on a 360×360 point radial lattice with a uniform mesh spacing of $\Delta r = 0.20$. Extensive calculations for each partial LS symmetry at specific incident electron energies were performed on massively parallel supercomputers. TIDW calculations [36] using HF removal energies were used to top up the TDCC calculations for $l \geqslant 8$.

In the RMPS calculations, the radial orbitals for the spectroscopic and pseudostates were determined using the atomic structure code AUTOSTRUCTURE [40]. Due to the large number of orbitals and configurations involved, we employed the Graphical AutoStructure Package (GASP) [41], a Java front end to AUTOSTRUCTURE. Spectroscopic orbitals were employed for the $1s$ to $5s$ subshells and they were calculated with a local potential that was determined using Slater-type orbitals. The higher Rydberg states and the target continuum were represented using nonorthogonal Laguerre pseudo-orbitals for all subshells from $5p$ to $13g$.

For electron-impact total ionization of the $2s$ and $2p$ subshells of the $1s^22s^22p^2\ {}^3P$ term, we made RMPS calculations using 1476 $LS\Pi$ terms coming from the 119 configurations of $1s^22s^22pnl$ ($n = 2$–13,$l = 0$–4), $1s^22s2p^2nl$ ($n = 2$–13,$l = 0$–4), and $1s^22p^3nl$ ($n = 3$–5,$l = 0$–4). For total ionization of only the $2p$ subshell of the $1s^22s2p^3\ {}^5S$, ${}^3D$, ${}^3P$ terms, we made an RMPS calculations using 937 $LS\Pi$ terms coming from the 49 configurations of $1s^22s2p^2nl$ ($n = 2$–12,$l = 0$–4). The first calculation involved around 4000 close-coupled channels; the second calculation involved around 2500 close-coupled channels. Both RMPS calculations were large scale involving repeated diagonalization of matrices of size $150\,000 \times 150\,000$, which were performed on massively parallel supercomputers. For the total cross section for the ground state, we calculated partial waves from $L = 0$ to $L = 12$ in the energy range from the first ionization threshold to just over 33 eV. The contributions from higher partial waves above $L = 12$ were then estimated for dipole transitions using the method originally described by Burgess [42] and for nondipole transitions assuming a geometric series in L, using energy ratios.

In the TIDW calculations, all energies and bound radial orbitals for C and C^+ were calculated using an HFR atomic structure code [34]. The configuration-average ionization potentials for the $2p$ and $2s$ subshells of the $1s^22s^22p^2$ ground configuration are 10.8 eV and 18.9 eV, respectively. The configuration-average ionization potentials for the $2p$ and $2s$ subshells of the $1s^22s2p^3$ excited configuration are 10.0 eV and 21.0 eV, respectively. The configuration-average ionization potentials for the $3s$, $2p$, and $2s$ subshells of the $1s^22s^22p3s$ excited configuration are 3.7 eV, 18.5 eV, and

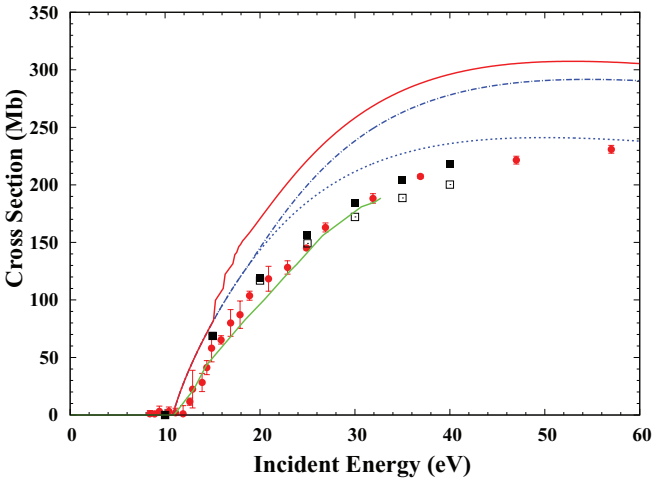

FIG. 1. (Color online) Electron-impact ionization cross section for the $1s^2 2s^2 2p^2$ ground configuration of neutral C: blue dotted and dash-dotted curves, TIDW($2p$) and TIDW($2s + 2p$) ionization, respectively; red solid curve, TIDW(tot) results for the the sum of the $2l$ ionization cross section and the excitation autoionization from $2s$ to $2p$, $3l$ ($l = 0$–2), and $4l$ ($l = 0$–3) subshells; black empty and filled squares, TDCC($2p$) and TDCC($2s + 2p$) ionization, respectively; green solid curve, RMPS results from the ^3P ground term only, which include both $2s$ and $2p$ ionization; and red circles with error bars, experimental measurements from the ^3P ground term only [14] (1 Mb = 1×10^{-18} cm^2).

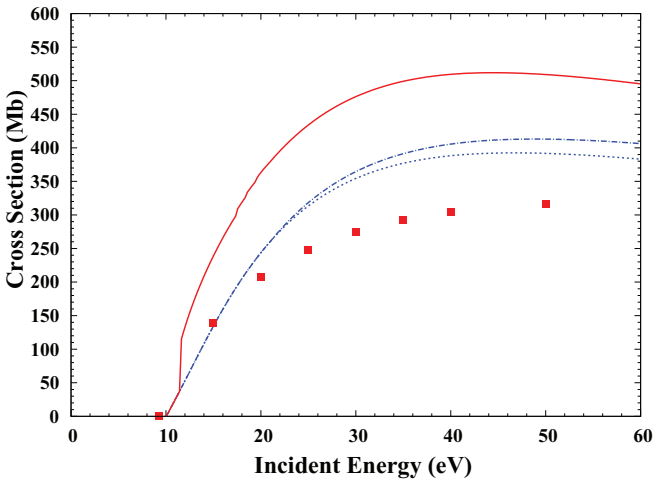

FIG. 2. (Color online) Electron-impact ionization cross section for the $1s^2 2s 2p^3$ excited configuration of C: blue dotted and dash-dotted curves, TIDW($2p$) and TIDW($2s + 2p$) results, respectively; red solid curve, TIDW(tot) results for the the sum of the $2l$ ionization cross sections and the excitation autoionization from $2s$ to $2p$, $3l$ ($l = 0$–2), and $4l$ ($l = 0$–3); red filled squares, TDCC results for the ionization of the $2p$ subshell (1 Mb = 1×10^{-18} cm^2).

25.3 eV, the configuration-average ionization potentials for the $3p$, $2p$, and $2s$ subshells of the $1s^2 2s^2 2p 3p$ excited configuration are 2.5 eV, 19.4 eV, and 26.0 eV, while the configuration-average ionization potentials for the $3d$, $2p$, and $2s$ subshells of the $1s^2 2s^2 2p 3d$ excited configuration are 1.6 eV, 20.0 eV, and 26.6 eV, which are all in reasonable agreement with the experimental values [39].

Partial waves of $l_i = 0$–50 and $l_f = 0$–50 were included in the TIDW sums of Eq. (6) to calculate $2s \rightarrow 2p,3l$ ($l = 0$–2),$4l$ ($l = 0$–3) excitations from both the $1s^2 2s^2 2p^2$ and $1s^2 2s 2p^3$ configurations, and $2p \rightarrow 3l$ ($l = 0$–2),$4l$ ($l = 0$–3) and $2s \rightarrow 2p,3l$ ($l = 0$–2),$4l$ ($l = 0$–3) excitations from the $1s^2 2s^2 2p 3l$ ($l = 0$–2) configurations. Partial waves of $l_i = 0$–50, $l_e = 0$–8, and $l_f = 0$–50 were included in the TIDW sums of Eq. (7) to calculate ionization of the $2l$ ($l = 0$–1) subshells of the $1s^2 2s^2 2p^2$ and $1s^2 2s 2p^3$ configurations, and ionization of the $2l$ ($l = 0$–1) and $3l$ ($l = 0$–2) subshells of the $1s^2 2s^2 2p 3l$ ($l = 0$–2) configurations.

A. C($1s^2 2s^2 2p^2$)

A comparison between perturbative (TIDW) and nonperturbative (TDCC, RMPS) results for the electron-impact ionization cross section of the $1s^2 2s^2 2p^2$ ground configuration with experimental measurements [14] is made in Fig. 1. The TDCC and TIDW methods were used to calculate direct-ionization contributions from the $2s$ and $2p$ subshells of the $1s^2 2s^2 2p^2$ ground configuration. The $2s$ subshell ionization affects the total cross section for incident electron energies above 19 eV. At 40 eV, the ionization cross section of the $2s$ subshell contributes 13% and 8% to the total TIDW and TDCC cross-section results, respectively. The TIDW method was used to calculate excitation-autoionization contributions for the $1s^2 2s^2 2p^2$ ground configuration. Contributions from the $2s \rightarrow 2p$, $2s \rightarrow 3l$ ($l = 0$–2) and $2s \rightarrow 4l$ ($l = 0$–3)

TABLE I. Comparison between the TDCC, TIDW, and RMPS results for the ionization of the $1s^2 2s^2 2p^2$ ground configuration of C (1 Mb = 1.0×10^{-18} cm^2).

	TDCC ($2p$)	TDCC ($2s$)	TIDW ($2p$)	TIDW ($2s$)	TIDW (ex)	RMPS
Threshold (eV)	10.0	18.0	10.8	18.9	15.2	10.0
Energy (eV)	Cross section (Mb)					
15.0	68.7		82.2			55.5
20.0	116.9	2.5	143.3	2.0	25.3	107.9
25.0	149.1	7.6	185.9	15.0	21.6	159.1
30.0	172.1	11.8	211.5	26.8	20.0	199.4
35.0	188.6	15.3	227.4	36.0	18.9	
40.0	200.2	18.3	235.9	42.3	18.0	
50.0	213.0	23.4	241.1	49.6	16.3	

TABLE II. Comparison between the TDCC, TIDW, and RMPS results for the ionization of the $1s^2 2s 2p^3$ excited configuration of C (1 Mb = 1.0×10^{-18} cm^2).

	TDCC ($2p$)	TIDW ($2p$)	TIDW ($2s$)	TIDW (ex)	RMPS ($2p$)
Threshold (eV)	9.3	10.0	21.0	11.5	10.8
Energy (eV)			Cross section (Mb)		
20.0	208.1	243.7		119.4	222.5
25.0	248.1	314.5	5.1	115.5	257.2
30.0	274.2	354.3	10.2	111.7	274.6
35.0	292.1	377.3	14.3	107.7	
40.0	304.0	388.2	17.3	104.0	
50.0	316.0	391.7	21.2	96.3	

excitations add up to 5% of the total TIDW results at 50 eV. The RMPS method was used to calculate the total-ionization cross section involving the $2s$ and $2p$ subshells from the $1s^2 2s^2 2p^2\ ^3P$ term, but not the ^1S and ^1D terms.

We present TDCC, TIDW, and RMPS numerical results for the electron-impact ionization of the $1s^2 2s^2 2p^2$ configuration in Table I. The RMPS result scaled to the configuration-average energy is in reasonable agreement with the sum of the $2s$ and $2p$ subshell TDCC results, indicating very little contribution from excitation-autoionization in the nonperturbative RMPS calculations. For LS-term selective ionization we recommend for $\sigma(C_i \rightarrow C_f)$ of Eq. (12) the sum of the TDCC cross sections for the $2p$ and $2s$ subshells found in columns 2 and 3 of Table I.

B. C($1s^2 2s 2p^3$)

A comparison between perturbative (TIDW) and nonperturbative (TDCC) results for the electron-impact ionization cross section of the $1s^2 2s 2p^3$ excited configuration is made in Fig. 2. The TDCC method was used to calculate the direct-ionization contributions from the $2p$ subshell, while the TIDW method was used to calculate direct-ionization contributions from the $2s$ and $2p$ subshells of the $1s^2 2s 2p^3$ excited configuration. The TIDW method overestimates the $2p$ direct ionization by 24% compared to the TDCC results at 50 eV, while the TIDW results for the $2s$ direct ionization contributes 5% to the TIDW direct ionization of the $2s$ and $2p$ subshells at the same energy. The TIDW method was used to calculate excitation-autoionization contributions for the $1s^2 2s 2p^3$ excited configuration. Contributions from the $2s \rightarrow 2p, 2s \rightarrow 3l$ ($l = 0$–2), and $2s \rightarrow 4l$ ($l = 0$–3) excitations add up to 19% of the total TIDW results at 50 eV.

We present TDCC, TIDW, and RMPS numerical results for the electron-impact ionization of the $1s^2 2s 2p^3$ configuration in Table II. The RMPS method was used to calculate the total-ionization cross section involving only the $2p$ subshell from the $1s^2 2s 2p^3\ ^5S, ^3P, ^3D$ terms, but not the $^3S, ^1P$, and ^1D terms. An LS-term averaged RMPS result is in reasonable agreement with the $2p$ subshell TDCC results. For LS-term selective ionization we recommend for $\sigma(C_i \rightarrow C_f)$ of Eq. (12) the sum of the TDCC cross section for the $2p$ subshell and the TIDW cross section for the $2s$ subshell found in columns 2 and 4 of Table II, with the addition of 50% of the TIDW excitation-autoionization contribution found in column 5 of Table II.

C. C($1s^2 2s^2 2p 3l$)

A comparison between perturbative (TIDW) and nonperturbative (TDCC) results for the electron-impact ionization cross sections of the $1s^2 2s^2 2p 3l$ excited configurations is made in Figs. 3–5. The TDCC method was used to calculate the direct-ionization contributions from the $3l$ subshells, while the TIDW method was used to calculate direct-ionization contributions from the $2s$, $2p$, and $3l$ subshells of the $1s^2 2s^2 2p 3l$ excited configurations. The TDCC calculations were carried out for all possible LS symmetries of the $3skl$, $3pkl$, and $3dkl$ coupled channels with $l \leqslant 7$. In order to check the convergence of the TDCC results, we studied the cross-section dependence on the angular momenta (l) at different incident electron energies. The TIDW results for $l \geqslant 8$ were used to top up the TDCC results for the $1s^2 2s^2 2p 3s$ excited configuration.

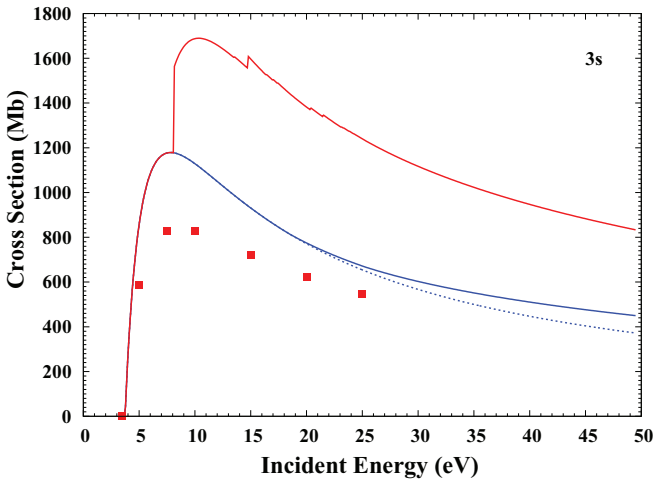

FIG. 3. (Color online) Electron-impact ionization cross section for the $1s^2 2s^2 2p 3s$ excited configuration of C: blue dotted and solid curves, TIDW($3s$) and TIDW ($3s + 2s + 2p$) results, respectively; red solid curve, TIDW(tot) results for the the sum of the $3s$ and $2l$ direct-ionization cross sections and the excitation autoionization from $2s$ and $2p$ to $3l$ ($l = 0$–2), $4l$ ($l = 0$–3), and $2s - 2p$; red filled squares, TDCC results for the ionization of the $3s$ subshell (1 Mb = 1×10^{-18} cm^2).

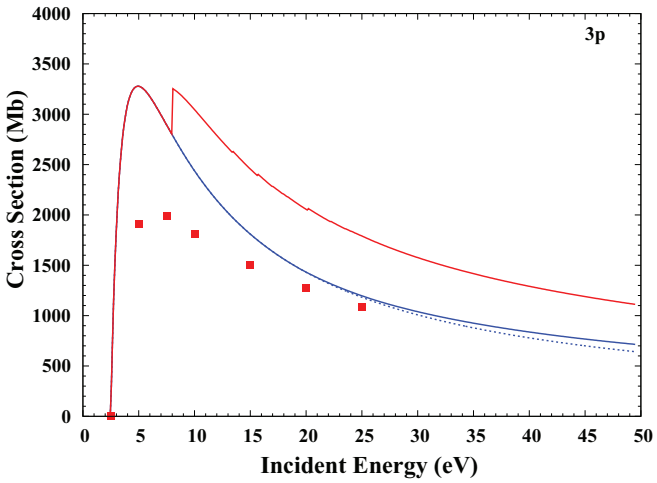

FIG. 4. (Color online) Electron-impact ionization cross section for the $1s^2 2s^2 2p 3p$ excited configuration of C: blue dotted and solid curves, TIDW($3p$) and TIDW($3p + 2s + 2p$) results, respectively; red solid curve, TIDW(tot) results for the the sum of the $3p$ and $2l$ direct-ionization cross sections and the excitation autoionization from $2s$ and $2p$ to $3l$ ($l = 0$–2), $4l$ ($l = 0$–3), and $2s - 2p$; red filled squares, TDCC results for the ionization of the $3p$ subshell (1 Mb = 1×10^{-18} cm^2).

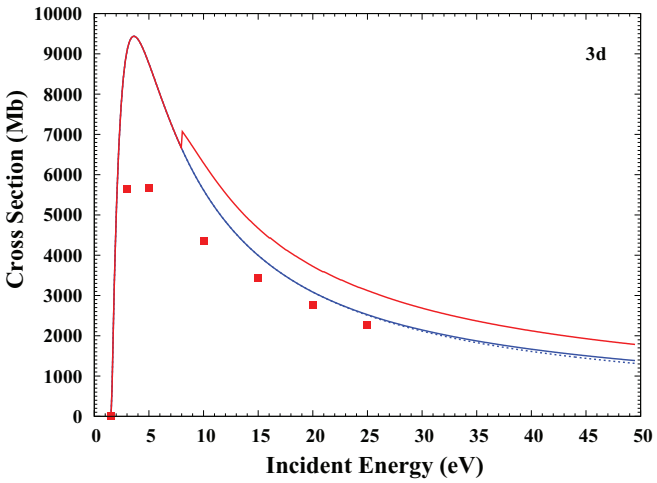

FIG. 5. (Color online) Electron-impact ionization cross section for the $1s^2 2s^2 2p 3d$ excited configuration of C: blue dotted and solid curves, TIDW($3d$) and TIDW($3d + 2s + 2p$) results, respectively; red solid curve, TIDW(tot) results for the the sum of the $3d$ and $2l$ direct-ionization cross sections and the excitation autoionization from $2s$ and $2p$ to $3l$ ($l = 0$–2), $4l$ ($l = 0$–3), and $2s - 2p$; red filled squares, TDCC results for the ionization of the $3d$ subshell (1 Mb = 1×10^{-18} cm^2).

On the other hand, extrapolations of the TDCC results were applied for $l = 8$–10 and $l = 8$–11 for the direct ionization of the $3p$ and $3d$ subshells, respectively. This produced partial-wave cross sections that are smoothly connected to the TIDW results at the higher l values for all the calculated energies. Then, the TIDW results were used to top up the final TDCC results for $l \geqslant 11$ and $l \geqslant 12$ for the $1s^2 2s^2 2p 3p$ and $1s^2 2s^2 2p 3d$ excited configurations, respectively. The TIDW method was used to calculate excitation-autoionization contributions for the $1s^2 2s^2 2p 3l$ excited configurations. Contributions from $2s \rightarrow 2p$, $2p \rightarrow 3l$ ($l = 0$–2), $2p \rightarrow 4l$ ($l = 0$–3), $2s \rightarrow 3l$ ($l = 0$–2), and $2s \rightarrow 4l$ ($l = 0$–3) excitations were calculated.

In Fig. 3 the peak of the TIDW results for $3s$ subshell direct ionization is 40% higher than the TDCC result. At 25 eV the peak of the TIDW results for the $3s$ and $2l$ subshell direct ionization is 20% higher than the TDCC results. At 50 eV, the TIDW excitation-autoionization contribution is 46% of the total TIDW cross section for the $1s^2 2s^2 2p 3s$ configuration. We present TDCC and TIDW numerical results for the electron-impact ionization of the $1s^2 2s^2 2p 3s$ configuration in Table III. For LS-term selective ionization we recommend for $\sigma(C_i \rightarrow C_f)$ of Eq. (12) the sum of the TDCC cross section for the $3s$ subshell and the TIDW cross sections for the $2l$ subshells found in columns 2, 4, and 5 of Table III, with the addition of 50% of the TIDW excitation-autoionization contribution found in column 6 of Table III.

In Fig. 4 the peak of the TIDW results for $3p$ subshell direct ionization is substantially higher than the TDCC results. At 25 eV the peak of the TIDW results for the $3p$ and $2l$ subshell direct ionization is 9% higher than the TDCC results. At 50 eV

TABLE III. Comparison between the TDCC and TIDW results for the ionization of the $1s^2 2s^2 2p 3s$ excited configuration of C (1 Mb = 1.0×10^{-18} cm^2).

	TDCC ($3s$)	TIDW ($3s$)	TIDW ($2p$)	TIDW ($2s$)	TIDW (ex)
Threshold (eV)	3.5	3.7	18.5	25.3	8.1
Energy (eV)			Cross section (Mb)		
5.0	585.6	856.6			
7.5	829.3	1177.4			
10.0	827.9	1128.9			558.8
15.0	720.2	931.0			638.3
20.0	620.8	771.2	3.5		607.5
25.0	545.1	654.3	17.3		553.7
30.0		567.1	29.1	6.4	514.6
35.0		500.1	37.8	13.6	463.4
40.0		447.0	43.8	19.6	436.6
45.0		404.1	47.8	24.3	406.7

TABLE IV. Comparison between the TDCC and TIDW results for the ionization of the $1s^2 2s^2 2p3p$ excited configuration of C (1 Mb = 1.0×10^{-18} cm^2).

	TDCC ($3p$)	TIDW ($3p$)	TIDW ($2p$)	TIDW ($2s$)	TIDW (ex)
Threshold (eV)	2.5	2.5	19.4	26.0	8.0
Energy (eV)			Cross section (Mb)		
5.0	1913.2	3277.4			
7.5	1988.7	2884.1			
10.0	1811.0	2438.5			607.9
15.0	1505.0	1809.7			646.1
20.0	1269.8	1430.7	1.5		623.8
25.0	1088.4	1182.3	14.8		594.2
30.0		1007.7	25.9	5.5	537.3
35.0		878.6	34.1	12.6	491.6
40.0		779.1	39.9	18.5	453.8
45.0		700.2	43.9	23.1	422.1

the TIDW excitation-autoionization contribution is 36% of the total TIDW cross section for the $1s^2 2s^2 2p3p$ configuration. We present TDCC and TIDW numerical results for the electron-impact ionization of the $1s^2 2s^2 2p3p$ configuration in Table IV. For LS-term selective ionization we recommend for $\sigma(C_i \rightarrow C_f)$ of Eq. (12) the sum of the TDCC cross section for the $3p$ subshell and the TIDW cross sections for the $2l$ subshells found in columns 2, 4, and 5 of Table IV, with the addition of 50% of the TIDW excitation-autoionization contribution found in column 6 of Table IV.

In Fig. 5 the peak of the TIDW results for $3d$ subshell direct ionization is substantially higher than the TDCC results. At 25 eV the TIDW results for the $3d$ and $2l$ subshell direct ionization is 11% higher than the TDCC results. At 50 eV the TIDW excitation-autoionization contribution is 22% of the total TIDW cross section for the $1s^2 2s^2 2p3d$ configuration. We present TDCC and TIDW numerical results for the electron-impact ionization of the $1s^2 2s^2 2p3d$ configuration in Table V. For LS-term selective ionization we recommend for $\sigma(C_i \rightarrow C_f)$ of Eq. (12) the sum of the TDCC cross section for the $3d$ subshell and the TIDW cross sections for the $2l$ subshells found in columns 2, 4, and 5 of Table V, with the addition of 50% of the TIDW excitation-autoionization contribution found in column 6 of Table V.

IV. SUMMARY

We have carried out extensive calculations for the electron-impact ionization cross sections of the $1s^2 2s^2 2p^2$ ground and $1s^2 2s 2p^3$, $1s^2 2s^2 2p3l$ ($l = 0$–2) excited configurations of C using the TDCC and TIDW methods. The RMPS method has been used for the ionization of the $1s^2 2s^2 2p^2\ ^3P$ ground and $1s^2 2s 2p^3\ ^5S$, ^3D, and ^3P excited terms. Ionization from both the $2s$ and $2p$ subshells was considered in our calculations for the ground configuration. The RMPS and the TDCC results are in reasonable agreement with the experimental cross sections [14], while the TIDW results are substantially higher. The TIDW method has been used to calculate the excitation autoionization from the $2s$ subshell for the $1s^2 2s^2 2p^2$ ground and the $1s^2 2s 2p^3$ excited configuration and from both the $2s$ and $2p$ subshells for the $1s^2 2s^2 2p3l$ ($l = 0$–2) excited configurations. For the ionization of the $1s^2 2s^2 2p3l$ ($l = 0$–2) excited configurations, the TDCC results are again found to be substantially lower than the TIDW results. Recommendations

TABLE V. Comparison between the TDCC and TIDW results for the ionization of the $1s^2 2s^2 2p3d$ excited configuration of C (1 Mb = 1.0×10^{-18} cm^2).

	TDCC ($3d$)	TIDW ($3d$)	TIDW ($2p$)	TIDW ($2s$)	TIDW (ex)
Threshold (eV)	1.5	1.6	20.0	26.6	8.0
Energy (eV)			Cross section (Mb)		
3.0	5637.3	9021.0			
5.0	5675.3	8757.9			
10.0	4360.9	5616.9			672.3
15.0	3424.3	3995.0			674.0
20.0	2771.4	3085.2			639.0
25.0	2270.6	2510.5	13.0		599.5
30.0		2116.0	24.0	4.6	542.0
35.0		1829.0	32.1	11.5	494.9
40.0		1611.0	37.9	17.3	456.8
45.0		1439.8	41.9	22	424.8

are made on the configuration-average total-ionization cross sections needed to extract *LS*-term selective-ionization cross sections needed for detailed modeling of the emission and transport of C in moderately dense plasmas. In the future, we plan to use the same methods to calculate electron-impact ionization cross sections for other atomic systems from ground and excited states.

ACKNOWLEDGMENTS

This work was supported in part by grants from the US Department of Energy and the US National Science Foundation. Computational work was carried out at the National Energy Research Scientific Computing Center in Oakland, California, and the National Institute for Computational Sciences in Knoxville, Tennessee.

[1] R. C. Isler, R. J. Colchin, N. H. Brooks, T. E. Evans, W. P. West, and D. Whyte, Phys. Plasmas **8**, 4470 (2001).
[2] R. C. Isler, N. H. Brooks, W. P. West, and A. G. McLean, Phys. Plasmas **14**, 012506 (2007).
[3] A. R. Field, C. Garcia-Rosales, G. Lieder, C. S. Pitcher, and R. Radtke, Nucl. Fusion **36**, 119 (1996).
[4] R. Schneider, D. Reiter, H. P. Zehrfeld, B. Braams, M. Baelmans, J. Geiger, H. Kastelewicz, J. Neuhauser, and R. Wunderlich, J. Nucl. Mater. **196-198**, 810 (1992).
[5] D. Reiter, J. Nucl. Mater. **196-198**, 80 (1992).
[6] A. V. Chankin, D. P. Coster, R. Dux, Ch. Fuchs, G. Haas, A. Herrmann, L. D. Horton, A. Kallenbach, M. Kaufmann, Ch. Konz, K. Lackner, C. Maggi, H. W. Müller, J. Neuhauser, R. Pugno, M. Reich, and W. Schneider, Plasma Phys. Control. Fusion **48**, 839 (2006).
[7] S. D. Loch, J. Colgan, M. C. Witthoeft, M. S. Pindzola, C. P. Ballance, D. M. Mitnik, D. C. Griffin, M. G. O'Mullane, N. R. Badnell, and H. P. Summers, At. Data Nucl. Data Tables **92**, 813 (2006).
[8] J. P. Allain, D. G. Whyte, and J. N. Brooks, Nucl. Fusion **44**, 655 (2004).
[9] J. G. Doyle, H. P. Summers, and P. Bryans, Astron. Astrophys. **430**, L29 (2005).
[10] G. Peach, J. Phys. B **3**, 328 (1970).
[11] G. Peach, J. Phys. B **4**, 1670 (1971).
[12] E. J. McGuire, Phys. Rev. A **1**, 267 (1971).
[13] K. Omidvar, H. L. Kyle, and E. C. Sullivan, Phys. Rev. A **5**, 1174 (1972).
[14] E. Brook, M. F. A. Harrison, and A. C. H. Smith, J. Phys. B **11**, 3115 (1978).
[15] W. Lotz, Astrophys. J. Suppl. **14**, 207 (1967).
[16] Y.-K. Kim and J.-P. Desclaux, Phys. Rev. A **66**, 012708 (2002).
[17] H. Suno and T. Kato, At. Data Nucl. Data Tables **92**, 407 (2006).
[18] A. K. F. Haque, M. A. Uddin, A. K. Basak, K. R. Karim, B. C. Saha, and F. B. Malik, Phys. Rev. A **73**, 052703 (2006).
[19] M. S. Pindzola, J. Colgan, F. Robicheaux, and D. C. Griffin, Phys. Rev. A **62**, 042705 (2000).
[20] J. A. Ludlow, S. D. Loch, M. S. Pindzola, C. P. Ballance, D. C. Griffin, C. P. Bannister, and M. Fogle, Phys. Rev. A **78**, 052708 (2008).
[21] C. P. Ballance, S. D. Loch, J. A. Ludlow, Sh. A. Abdel-Naby, and M. S. Pindzola, Phys. Rev. A **84**, 062713 (2011).
[22] M. Fogle, E. M. Bahati, M. E. Bannister, C. R. Vane, S. D. Loch, M. S. Pindzola, C. P. Ballance, R. D. Thomas, V. Zhaunerchyk, P. Bryans, W. Mitthumsiri, and D. W. Savin, Astrophys. J. Suppl. Ser. **175**, 543 (2008).
[23] S. D. Loch, M. Witthoeft, M. S. Pindzola, I. Bray, D. V. Fursa, M. Fogle, R. Schuch, P. Glans, C. P. Ballance, and D. C. Griffin, Phys. Rev. A **71**, 012716 (2005).
[24] D. M. Mitnik, M. S. Pindzola, D. C. Griffin, and N. R. Badnell, J. Phys. B **32**, L479 (1999).
[25] M. S. Pindzola, C. P. Ballance, and S. D. Loch, Phys. Rev. A **83**, 062705 (2011).
[26] D. C. Griffin and M. S. Pindzola, Adv. Atm. Mol. **54**, 203 (2006).
[27] C. F. Fischer, *The Hartree-Fock Method for Atoms* (Wiley, New York, 1977).
[28] K. Bartschat, E. T. Hudson, M. P. Scott, P. G. Burke, and V. M. Burke, J. Phys. B **29**, 115 (1996).
[29] T. W. Gorczyca and N. R. Badnell, J. Phys. B **30**, 3897 (1997).
[30] D. M. Mitnik, D. C. Griffin, C. P. Ballance, and N. R. Badnell, J. Phys. B **36**, 717 (2003).
[31] C. P. Ballance and D. C. Griffin, J. Phys. B **37**, 2943 (2004).
[32] K. A. Berrington, W. B. Eissner, and P. H. Norrington, Comput. Phys. Commun. **92**, 290 (1995).
[33] M. S. Pindzola, D. C. Griffin, and C. Bottcher, in *Atomic Processes in Electron-Ion and Ion-Ion Collisions*, edited by F. B. Plenum, NATO Advanced Study Institute, Series B: Physics, (Plenum, New York, 1986), Vol. 145, p. 75.
[34] R. D. Cowan, *The Theory of Atomic Structure and Spectra* (University of California, Berkeley, CA, 1981).
[35] J. Botero and J. H. Macek, J. Phys. B **24**, L405 (1991).
[36] S. M. Younger, Phys. Rev. A **24**, 1278 (1981).
[37] D. H. Sampson, Phys. Rev. A **34**, 986 (1986).
[38] M. S. Pindzola, F. Robicheaux, S. D. Loch, J. C. Berengut, T. Topcu, J. Colgan, M. Foster, D. C. Griffin, C. P. Ballance, D. R. Schultz, T. Minami, N. R. Badnell, M. C. Witthoeft, D. R. Plante, D. M. Mitnik, J. A. Ludlow, and U. Kleiman, J. Phys. B **40**, R39 (2007).
[39] See http://physics.nist.gov/PhysRefData/ASD/levels_form.html.
[40] N. R. Badnell, J. Phys. B **30**, 1 (1997).
[41] See http://connorb.freeshell.org/gasp.
[42] A. Burgess, J. Phys. B **7**, L364 (1970).